Applied Mathematics & Information Sciences
An International Journal

http://dx.doi.org/10.18576/amis/200503

Cascaded Frequency-Response Synthesis for Enhanced Side-Lobe Rejection and 3-dB Bandwidth Sharpening in Surface Acoustic Wave Filters

Haitham Issa[1], *Hani Attar*[1], *Jafar Ababneh*[2], *Zakaria Che Muda*[3], *Ismail A. M. Elhaty*[4], *Eman Salah Abass* [5], *and Ramy M. Bahy*[6,*]

[1]Department of Electrical Engineering, Faculty of Engineering, Zarqa University, Zarqa 132222, Jordan
[2]Faculty of Information Technology, Cyber Security, Zarqa University, Zarqa 132222, Jordan
[3]Department of Civil Engineering, Faculty of Engineering and Quantity Surveying, INTI International University, 71800 Nilai, Malaysia
[4]Department of Nutrition and Dietetics, Faculty of Health Sciences, Istanbul Gelisim University, Istanbul, Turkey
[5]Faculty of Computer and Artificial Intelligence, AlRyada University, Sadat City, Egypt
[6]Technical Research Center, Cairo, Egypt

Received: 7 Jul. 2026, Revised: 8 Aug. 2026, Accepted: 23 Aug. 2026
Published online: 1 Sep. 2026

Abstract: This paper presents a cascaded frequency-response approach for enhancing side-lobe rejection and sharpening the 3-dB bandwidth of surface acoustic wave (SAW) filters. The method is applied to a uniformly apodized rectangular-window SAW filter composed of a 7-electrode input interdigital transducer (IDT) and a 40-electrode output IDT. The individual IDT responses are first modeled using the delta-function approximation and simulated in MATLAB. The baseline transfer response is then iteratively cascaded by repeated multiplication with the output-IDT response, generating a sequence of composite responses up to 50 cascade orders. For each cascade order, the center frequency, peak response level, insertion-loss magnitude, side-lobe rejection, and 3-dB bandwidth are extracted and analyzed. The simulated results show that the center frequency remains nearly constant at approximately 162 MHz after the first cascade, while the side-lobe rejection increases almost linearly with cascade order. Specifically, the side-lobe rejection improves from 8.24 dB for the baseline response to 575.8 dB after 50 cascades. In contrast, the 3-dB bandwidth decreases nonlinearly from 8.70 MHz to 0.549 MHz over the same range. A linear regression model is developed for predicting side-lobe rejection, while Gaussian, polynomial, and power-law models are evaluated for bandwidth prediction. The extracted models provide compact design equations for estimating the cascade order required to satisfy a target side-lobe rejection or bandwidth. The results also reveal a significant trade-off between selectivity improvement and insertion-loss degradation, as the peak response level decreases from approximately -11.31 dB to -305.50 dB after 50 cascades. The proposed method therefore provides an ideal frequency-response synthesis and design-screening framework that can contribute to process innovation and product innovation in high-selectivity RF and SAW-filter components. By supporting improved frequency selectivity and reliable front-end filtering for modern communication and sensing systems, the approach is relevant to the development of resilient infrastructure and broader infrastructural development in advanced wireless technologies. The method also provides a computationally efficient route for early-stage design evaluation that may support future manufacturing innovation, although practical realization requires dynamic-range-aware design, physical cascading analysis, and validation using higher-order acoustic models or measurements. These contributions align the work with United Nations Sustainable Development Goal 9, Industry, Innovation and Infrastructure.

Keywords: Surface acoustic wave filter, interdigital transducer, delta-function model, cascaded frequency response, side-lobe rejection, 3-dB bandwidth, insertion loss, narrowband filter.

1 Introduction

Surface acoustic wave (SAW) filters are widely used in radio-frequency (RF), intermediate-frequency (IF), sensing, and communication systems because they provide compact size, high frequency selectivity, compatibility with planar fabrication, and good reproducibility [1–4]. Their operating principle is based

* Corresponding author e-mail: ramymbahy@gmail.com

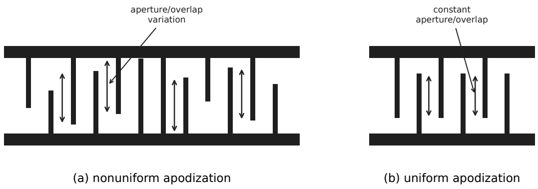

Fig. 1: Representative IDT structures: (a) nonuniformly apodized structure and (b) uniformly apodized structure.

on the piezoelectric conversion between electrical and acoustic energy using interdigital transducers (IDTs). This concept originates from the direct excitation of surface elastic waves by periodic electrodes on a piezoelectric substrate [5]. In a conventional two-port SAW filter, the input IDT converts the applied electrical signal into a surface acoustic wave, which propagates along the substrate and is then reconverted into an electrical signal by the output IDT. Therefore, the transfer response of the filter is mainly determined by the geometrical design, weighting function, and relative placement of the input and output IDTs [6–8].

The IDT geometry can be interpreted as a spatially sampled representation of the desired impulse response. Consequently, the frequency response of a SAW filter is strongly affected by the number of electrodes, acoustic wavelength, electrode width, aperture, metallization ratio, transducer spacing, and apodization profile [6, 7]. Figure 1 illustrates two representative IDT configurations: a nonuniformly apodized IDT and a uniformly apodized IDT. In nonuniformly apodized structures, the electrode overlap is varied along the transducer aperture to shape the impulse response and reduce side-lobe levels. In uniformly apodized structures, all electrode overlaps are kept constant, resulting in a rectangular-window response that is simpler to implement but generally produces higher side lobes.

Uniformly apodized, or rectangular-window, IDTs are attractive because of their simple layout, straightforward fabrication, and direct analytical interpretation. However, rectangular weighting is known to produce relatively high side-lobe levels, as also observed in classical window-based spectral analysis [9]. In SAW-filter applications, these side lobes can limit out-of-band rejection, adjacent-channel suppression, and overall frequency selectivity. Therefore, improving side-lobe rejection while reducing the 3-dB bandwidth remains an important objective in SAW-filter design, especially for narrowband and highly selective systems.

Several approaches have been used to improve SAW-filter selectivity, including electrode apodization, withdrawal weighting, split-finger electrodes, unidirectional transducers, resonator-based configurations, and multi-stage filter structures [2, 6–8, 10–12]. These techniques can provide substantial improvements in frequency response, but they may also increase design complexity, fabrication sensitivity, insertion loss, or optimization time. For this reason, compact analytical and simulation-based methods that can predict the trade-off between side-lobe suppression, bandwidth sharpening, and insertion-loss degradation remain useful during early-stage filter design.

SAW-filter responses can be analyzed using different levels of modeling complexity. Simplified approaches include impulse-response and delta-function models, while more complete approaches include equivalent-circuit models, coupling-of-modes analysis, P-matrix methods, and finite-element simulation [6, 8, 13–15]. In this work, the delta-function model is adopted because it provides a direct first-order relationship between the IDT electrode-edge distribution and the resulting frequency response. In this model, each electrode edge is represented as a discrete acoustic or electric-field source, and the overall IDT response is obtained by summing the contributions of all edge sources and applying the Fourier-transform relationship. Although the model does not fully include practical second-order effects such as electromagnetic feedthrough, electrode reflections, diffraction, impedance loading, propagation loss, and triple-transit interference, it is suitable for studying the fundamental response-shaping effect produced by repeated frequency-domain multiplication [6, 7].

This paper investigates a cascaded frequency-response methodology for improving the selectivity of a uniformly apodized rectangular-window SAW filter. The baseline filter consists of a 7-electrode input IDT and a 40-electrode output IDT. The individual input- and output-IDT responses are first calculated using the delta-function approximation. The baseline two-port response is then obtained from the product of the two IDT responses. After that, the composite response is repeatedly multiplied by the output-IDT response to generate higher-order cascaded responses. The Kth cascaded response is expressed as

$$H_{c,K}(f) = H_{in}(f)\,[H_{out}(f)]^{K}, \qquad (1)$$

where $H_{in}(f)$ and $H_{out}(f)$ denote the frequency responses of the input and output IDTs, respectively, $H_{c,K}(f)$ is the Kth cascaded composite response, and K is the cascade order. This repeated multiplication progressively attenuates frequency components away from the main lobe, thereby increasing side-lobe rejection and narrowing the 3-dB bandwidth.

The objective of this work is not to introduce a new IDT geometry or add new physical filter stages, but to quantify how repeated frequency-response cascading affects the main performance parameters of a uniformly apodized SAW filter. The center frequency, peak response level, side-lobe rejection, and 3-dB bandwidth are extracted for cascade orders up to 50. Additional high-order simulations are used to illustrate the model-predicted narrowband and ultra-narrowband behavior. The extracted data are then used to develop compact regression models that relate cascade order to side-lobe rejection and 3-dB bandwidth. These models provide practical early-stage design tools for estimating the cascade order required to approach a target rejection level or bandwidth.

The novelty of this work lies in quantifying the selectivity–loss scaling laws produced by repeated output-IDT spectral weighting in a uniformly apodized SAW-filter response. Although transfer-function multiplication is a standard property of cascaded linear systems, its systematic use here provides compact predictive relationships between cascade order, side-lobe rejection, 3-dB bandwidth, center-frequency stability, and insertion-loss penalty for a rectangular-window SAW response. Thus, the contribution is not a new electrode layout, but a response-synthesis framework and design-screening method for estimating the achievable selectivity improvement before moving to higher-fidelity physical modeling.

The main contributions of this paper are summarized as follows:

–A cascaded frequency-response formulation is applied to a uniformly apodized rectangular-window SAW filter using the delta-function model.
–The influence of cascade order on center frequency, peak response level, side-lobe rejection, and 3-dB bandwidth is systematically evaluated.
–A linear predictive model is extracted for side-lobe rejection as a function of cascade order.
–Nonlinear regression models are developed for predicting the reduction in 3-dB bandwidth with increasing cascade order.
–The selectivity improvement is discussed together with the associated insertion-loss penalty, providing a practical interpretation of the proposed response-cascading method.

The comparison in Table 1 shows that the proposed approach should be viewed as complementary to physical SAW-filter optimization methods, not as a replacement for apodization, resonator design, or full multi-stage implementation.

The remainder of this paper is organized as follows. Section 2 presents the frequency-response formulation of bidirectional SAW filters and reviews the delta-function model. Section 3 describes the uniformly apodized SAW-filter design used in the simulations. Section 4 introduces the proposed cascaded frequency-response methodology. Section 5 defines the simulation setup and performance metrics. Section 6 presents the simulated frequency responses and extracted parameters. Section 7 develops the regression models for side-lobe rejection and 3-dB bandwidth. Section 8 discusses the selectivity–loss trade-off and practical interpretation of the results. Section 9 presents the narrowband and ultra-narrowband

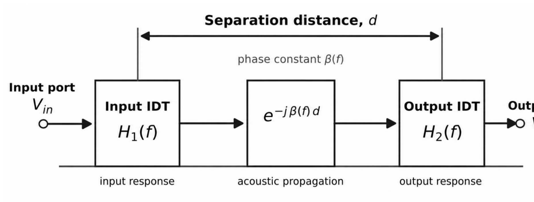

Fig. 2: Block diagram of the input and output IDTs separated by an effective propagation distance $x(f)$.

implications. Section 10 summarizes the main limitations and future work, and Section 11 concludes the paper.

2 SAW-Filter Frequency-Response Theory

2.1 Frequency Response of a Bidirectional SAW Filter

The operation of a surface acoustic wave (SAW) filter is based on the electromechanical conversion between an electrical signal and an acoustic surface wave through interdigital transducers (IDTs). Since the first demonstration of direct piezoelectric coupling to surface elastic waves using periodic electrodes [5], the IDT has become the fundamental building block of SAW delay lines, transversal filters, resonators, and RF front-end filtering devices [6–8]. In a two-port SAW filter, the input IDT converts the applied voltage into a propagating acoustic wave, whereas the output IDT converts the received acoustic wave back into an electrical voltage. Therefore, the filter transfer function is governed primarily by the frequency responses of the input and output IDTs and by the acoustic propagation phase between them.

For an ideal bidirectional SAW filter, the overall voltage transfer function can be written as [6–8]

$$H(f) = \frac{V_{\text{out}}(f)}{V_{\text{in}}(f)} = H_1(f)H_2^*(f)\exp[-j\beta(f)x(f)], \quad (2)$$

where $V_{\text{in}}(f)$ and $V_{\text{out}}(f)$ are the input and output voltages in the frequency domain, respectively. The terms $H_1(f)$ and $H_2(f)$ denote the input- and output-IDT frequency responses, respectively, and $H_2^*(f)$ is the complex conjugate of the output-IDT response. The acoustic phase constant is

$$\beta(f) = \frac{2\pi}{\lambda} = \frac{2\pi f}{v_{\text{SAW}}}, \quad (3)$$

where λ is the acoustic wavelength and v_{SAW} is the SAW phase velocity. The term $x(f)$ represents the effective acoustic propagation distance between the input and output transducers.

When the separation between the input and output IDTs is fixed, the effective propagation distance can be

Table 1: Comparison of SAW-filter response-shaping methods and their relation to the proposed cascaded frequency-response approach.

Method	Advantage	Limitation	Relation to this work
Electrode apodization	Reduces side lobes physically	May broaden the main lobe and increase layout complexity	The proposed method studies repeated spectral weighting instead of changing aperture weights
Withdrawal weighting	Improves response shaping	More fabrication-sensitive	The proposed method avoids new geometry but introduces a loss penalty
Split-finger IDT	Reduces reflections	Larger layout and more complex design	The present model does not yet include reflection suppression
Resonator-based SAW filters	High practical selectivity	Requires more complete physical modeling	The proposed method is simpler but currently idealized
Physical multi-stage SAW filters	Real transfer-function cascading	Loading, matching, and accumulated loss	Closest physical analogue to the proposed mathematical cascade

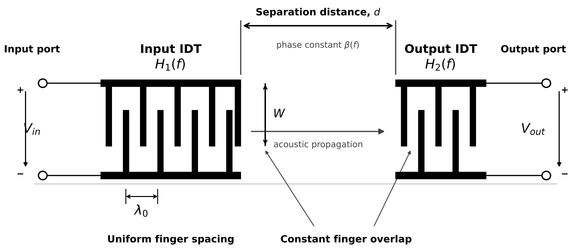

Fig. 3: Input and output IDTs with a fixed separation distance d.

approximated by a constant distance d, measured between the reference centers of the two transducers. In this case, (2) becomes

$$H(f) = H_1(f)H_2^*(f)\exp[-j\beta(f)d]. \tag{4}$$

Under the lossless-propagation approximation, the exponential term in (4) contributes only a frequency-dependent phase shift and does not modify the magnitude response. Therefore, the magnitude selectivity of the ideal two-port filter is mainly determined by the product of the input- and output-IDT responses:

$$|H(f)| = |H_1(f)|\,|H_2(f)|. \tag{5}$$

This relationship is important for the cascaded-response method developed in this paper, because repeated multiplication by the output-IDT response progressively suppresses spectral components away from the main lobe.

The frequency response and impulse response of a linear SAW transversal filter are related through the Fourier-transform pair [6, 7, 13]

$$H(f) = \int_{-\infty}^{\infty} h(t)\exp(-j2\pi ft)\,dt, \tag{6}$$

and

$$h(t) = \int_{-\infty}^{\infty} H(f)\exp(j2\pi ft)\,df, \tag{7}$$

where $h(t)$ is the impulse response and $H(f)$ is the corresponding frequency response. In SAW transversal-filter design, the IDT electrode pattern can be interpreted as a spatially sampled representation of the desired impulse response. Consequently, the geometry and weighting of the IDT determine the frequency-domain characteristics of the device, including center frequency, insertion loss, side-lobe rejection, and 3-dB bandwidth [6–8].

2.2 Delta-Function Model

Several analytical and numerical models can be used to analyze IDT-based SAW devices, including the delta-function model, equivalent-circuit models, coupling-of-modes models, P-matrix formulations, and finite-element methods [6, 8, 13, 14, 16]. The present work adopts the delta-function model because it provides a direct and computationally efficient first-order description of the IDT frequency response.

In the delta-function model, each electrode edge is represented as an elemental point source of electric field or charge distribution. When a voltage is applied across the IDT, opposite-polarity electrodes generate charge accumulation at their edges. These edge charges excite acoustic waves whose amplitudes and phases depend on the electrode positions. The total transducer response is obtained by summing the contribution of all electrode-edge sources and then transforming the resulting spatial impulse distribution into the frequency domain [6–8, 16, 17].

For an IDT with P effective edge sources located at positions x_p, the spatial source distribution may be written in simplified form as

$$s(x) = \sum_{p=1}^{P} A_p \delta(x - x_p), \tag{8}$$

where A_p is the signed amplitude associated with the pth electrode edge and $\delta(\cdot)$ is the Dirac delta function. The corresponding frequency response can then be approximated by

$$H_{\mathrm{IDT}}(f) \propto \sum_{p=1}^{P} A_p \exp\left(-j\frac{2\pi f}{v_{\mathrm{SAW}}}x_p\right). \tag{9}$$

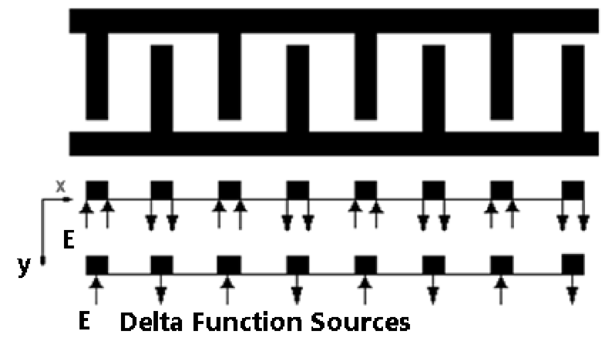

Fig. 4: Delta-function representation of an IDT in a SAW filter.

Equation (9) shows that the IDT response is determined by the relative positions and polarities of the electrode edges. For a uniformly apodized rectangular-window IDT, the amplitudes A_p are constant in magnitude, whereas their signs are determined by the alternating electrode polarity. As a result, the response exhibits a main lobe around the synchronous frequency and side lobes whose levels are governed by the effective rectangular spatial weighting.

The delta-function model is particularly suitable for the present study because the objective is to examine how repeated frequency-response multiplication affects the main response metrics of a uniformly apodized SAW filter. Although the model is simplified, it captures the dominant relationship between IDT geometry and magnitude response. It therefore provides a useful basis for estimating insertion loss as a function of frequency and for evaluating the relative changes in side-lobe rejection and 3-dB bandwidth caused by the proposed cascaded-response process [6, 7].

2.3 Second-Order Effects

The ideal formulation in (2)–(4) assumes that the SAW device behaves as a linear transversal filter with negligible parasitic coupling and ideal acoustic propagation. In practical devices, however, the measured response may deviate from the ideal response because of several second-order effects. The most important mechanisms include electromagnetic feedthrough, triple-transit interference, electrode finger reflections, acoustic diffraction, bulk-wave excitation, impedance loading, and propagation loss [6, 8, 13, 18, 19].

Electromagnetic feedthrough results from direct electrical coupling between the input and output ports and can introduce a spurious signal that bypasses the acoustic path. Triple-transit interference is caused by multiple acoustic reflections between the transducers, producing delayed echoes that distort the passband and ripple characteristics. Electrode finger reflections arise from acoustic impedance discontinuities at the metallized electrode edges and become increasingly important in reflective or resonant SAW structures. Diffraction and bulk-wave radiation can also reduce the accuracy of the ideal transversal-filter response, especially when the acoustic aperture, substrate properties, and propagation path are not optimized.

In the present work, the delta-function model is used as the primary simulation framework, and the focus is placed on the effect of cascaded frequency-response multiplication on the ideal magnitude response. A fixed triple-transit-interference loss term is included in the simulation assumptions, whereas the remaining second-order mechanisms are not explicitly modeled. This choice allows the proposed cascaded-response trend to be isolated and evaluated without introducing additional structural modifications or fitting parameters. More complete physical modeling, including electromagnetic feedthrough, electrode reflections, acoustic diffraction, impedance loading, and propagation loss, is therefore identified as an important direction for future refinement.

3 Uniformly Apodized SAW-Filter Design

The frequency response of a SAW filter is strongly dependent on the geometrical configuration of its interdigital transducers (IDTs), including the acoustic wavelength, electrode width, number of electrodes, aperture weighting, and spacing between the input and output transducers [6–8, 13]. In the present study, a uniformly apodized rectangular-window SAW-filter structure is considered in order to provide a simple and controlled baseline for evaluating the proposed cascaded frequency-response method [10, 15]. The use of a rectangular, uniformly weighted IDT is advantageous because it provides a direct relationship between the electrode distribution and the resulting frequency response. However, rectangular weighting is also known to produce relatively high side-lobe levels, as expected from classical window theory [9]. This makes the structure suitable for studying side-lobe-rejection improvement through response cascading.

The investigated filter consists of one input IDT and one output IDT separated by a fixed acoustic propagation distance, as shown in Fig. 5. Both transducers are implemented using uniformly apodized rectangular electrode structures. In this configuration, all electrode fingers have constant overlap, and no amplitude tapering is applied across the aperture. Therefore, the design corresponds to a uniformly weighted transversal SAW-filter structure [6, 7].

The input IDT contains $N = 7$ electrodes with an electrode width of $5\,\mu$m. Assuming the conventional quarter-wavelength electrode relationship, the corresponding acoustic wavelength is

$$\lambda_1 = 4w_1, \tag{10}$$

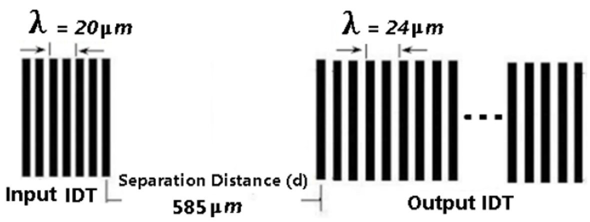

Fig. 5: Uniformly apodized SAW filter using rectangular-window input and output IDT structures.

Table 2: Main design parameters of the uniformly apodized SAW filter.

Parameter	Input IDT	Output IDT
Number of electrodes	7	40
Electrode width	5 μm	6 μm
Acoustic wavelength	20 μm	24 μm
Nominal center frequency	194.3 MHz	161.92 MHz
SAW velocity	3886 m s^{-1}	
IDT separation distance	585 μm	
Apodization type	Uniform rectangular weighting	

where w_1 is the input-electrode width. Thus, the input-IDT wavelength is 20 μm. Similarly, the output IDT contains $M = 40$ electrodes with an electrode width of 6 μm, corresponding to an acoustic wavelength of

$$\lambda_2 = 4w_2 = 24\,\mu\text{m}, \tag{11}$$

where w_2 is the output-electrode width.

For a periodic IDT, the synchronous or nominal center frequency is determined by the acoustic velocity and the acoustic wavelength [5–7]. It is given by

$$f_0 = \frac{v_{\text{SAW}}}{\lambda}, \tag{12}$$

where v_{SAW} is the assumed surface-acoustic-wave phase velocity and λ is the acoustic wavelength. In this work, the effective SAW velocity is taken as 3886 m s^{-1}. Therefore, the nominal synchronous frequency of the input IDT is calculated as

$$f_{01} = \frac{3886}{20 \times 10^{-6}} = 194.3\,\text{MHz}, \tag{13}$$

whereas the nominal synchronous frequency of the output IDT is

$$f_{02} = \frac{3886}{24 \times 10^{-6}} = 161.92\,\text{MHz}. \tag{14}$$

The separation distance between the input and output IDTs is fixed at 585 μm. This distance introduces a propagation phase term in the overall transfer function, as discussed in Section 2. Under the ideal lossless-propagation approximation, this separation mainly affects the phase response, while the magnitude response is governed by the product of the input- and output-IDT responses [6, 8]. Since the objective of this work is to examine side-lobe rejection and 3-dB bandwidth sharpening, the magnitude response is used as the primary performance indicator.

The main design parameters of the uniformly apodized SAW filter are summarized in Table 2. The unequal input and output acoustic wavelengths intentionally produce different nominal IDT synchronous frequencies. As will be shown in the simulation results, the composite response is dominated by the output-IDT response and exhibits a main passband close to 162 MHz. This makes the output IDT the main response-shaping element in the subsequent cascaded-frequency-response process.

The baseline frequency response is obtained by calculating the individual input- and output-IDT responses using the delta-function model and then multiplying them to form the two-port response. This baseline response is later used as the first stage of the proposed cascaded-response procedure. Specifically, after obtaining the initial response, the composite response is repeatedly multiplied by the output-IDT response in order to sharpen the main lobe and suppress the side lobes. Thus, the design in this section provides the reference geometry from which all subsequent cascaded responses, bandwidth values, side-lobe-rejection values, and insertion-loss trends are extracted.

4 Proposed Cascaded Frequency-Response Methodology

The frequency response of a two-port SAW filter is determined by the combined effect of the input and output interdigital transducers (IDTs) and the acoustic propagation path between them [6–8, 13]. For a linear time-invariant system, cascading frequency-selective stages corresponds to multiplication of their transfer functions in the frequency domain. In conventional SAW-filter analysis, the overall response is obtained from the product of the individual transducer responses together with the acoustic propagation phase term [6, 7]. In the present work, this principle is extended in a systematic way to investigate how repeated multiplication by the output-IDT response affects the selectivity of a uniformly apodized rectangular-window SAW filter.

It should be emphasized that the proposed method is formulated as a *frequency-response synthesis and analysis procedure*. In other words, the study does not introduce an additional physical transducer structure or a new fabricated multi-stage device. Instead, it repeatedly applies the output-IDT response in the frequency domain in order to quantify the resulting changes in the composite magnitude response. This approach provides a simple analytical framework for evaluating the evolution of the

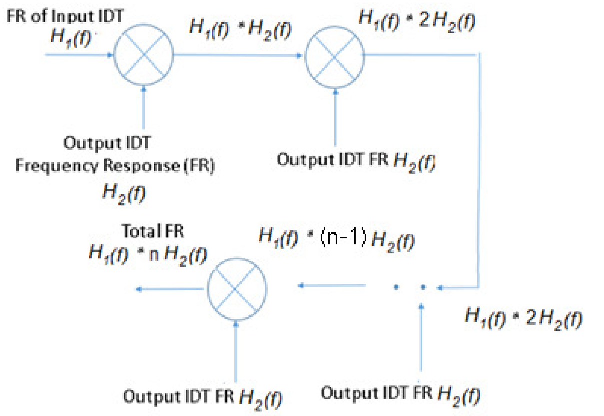

Fig. 6: Schematic diagram of the proposed multi-response SAW-filter design process.

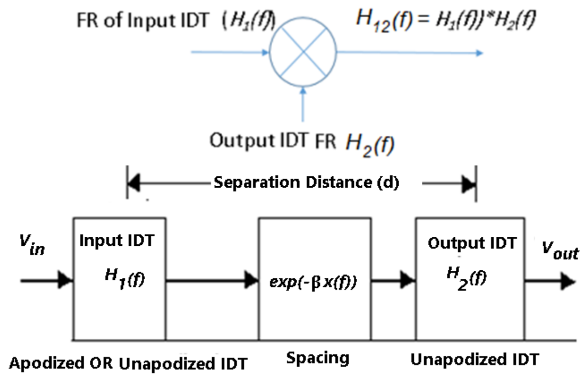

Fig. 7: Block diagram of the baseline SAW-filter response, $H_{c,1}(f)$, also denoted as $H_{12}(f)$ in the figure.

center frequency, insertion loss, side-lobe rejection, and 3-dB bandwidth as the effective cascade order increases.

4.1 Baseline Composite Response

The procedure begins by calculating the individual frequency responses of the input and output IDTs, denoted by $H_{\text{in}}(f)$ and $H_{\text{out}}(f)$, respectively, using the delta-function model described in Section 2. Since the present analysis is focused on the magnitude response, the propagation phase factor is omitted from the cascade formulation because it does not affect the response magnitude under the ideal lossless-propagation assumption [6, 8]. Accordingly, the first composite response, corresponding to the basic two-port SAW filter, is written as

$$H_{c,1}(f) = H_{\text{in}}(f)H_{\text{out}}(f). \tag{15}$$

Equation (15) represents the baseline SAW-filter response and corresponds to the first effective frequency-response cascade order, $K = 1$. Physically, this response corresponds to the initial combination of the input-IDT excitation function and the output-IDT reception function. Because the output IDT in the present design contains a larger number of electrodes and exhibits a narrower response than the input IDT, it plays the dominant role in shaping the overall passband.

Figure 6 summarizes the overall methodology. The process starts from the baseline two-port response and then proceeds through repeated frequency-domain multiplication by the output-IDT response. This repeated multiplication gradually suppresses the out-of-band components and side lobes, thereby sharpening the main lobe of the composite response.

4.2 Iterative Cascading Procedure

After obtaining the baseline response $H_{12}(f)$, the output-IDT response is applied again to generate a higher-order cascaded response. The second-order cascaded response is given by

$$H_{c,2}(f) = H_{c,1}(f)H_{\text{out}}(f). \tag{16}$$

which can also be written as

$$H_{c,2}(f) = H_{\text{in}}(f)\left[H_{\text{out}}(f)\right]^2. \tag{17}$$

Similarly, the third-order cascaded response becomes

$$H_{c,3}(f) = H_{c,2}(f)H_{\text{out}}(f). \tag{18}$$

or equivalently,

$$H_{c,3}(f) = H_{\text{in}}(f)\left[H_{\text{out}}(f)\right]^3. \tag{19}$$

The notations $H_{12}(f)$, $H_{122}(f)$, and $H_{1222}(f)$ are used only in the figures to indicate the first, second, and third composite responses, respectively.

Thus, each additional cascade step applies one more multiplication by the output-IDT response. This operation effectively strengthens the spectral weighting imposed by the output transducer. Since the magnitude of $|H_{\text{out}}(f)|$ is largest around the main lobe and smaller away from it, repeated multiplication increasingly attenuates off-peak frequency components. As a result, the main lobe becomes narrower, while the side lobes are progressively reduced. This behavior is analogous, in a frequency-domain sense, to repeatedly enforcing the spectral selectivity of the output transducer [6, 7].

Figures 7–9 illustrate the first three stages of the process. Figure 7 corresponds to the baseline two-port response, Fig. 8 shows the first additional cascade with the output-IDT response, and Fig. 9 shows the next cascade stage. These diagrams visually clarify how the proposed response-synthesis method is constructed from repeated application of the same output spectral response.

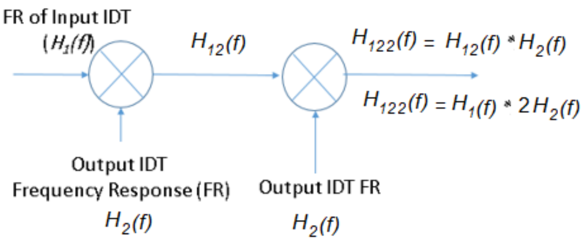

Fig. 8: Block diagram of the second-order cascaded response, $H_{c,2}(f)$, also denoted as $H_{122}(f)$ in the figure.

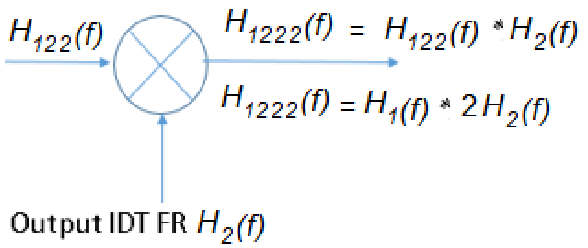

Fig. 9: Block diagram of the third-order cascaded response, $H_{c,3}(f)$, also denoted as $H_{1222}(f)$ in the figure.

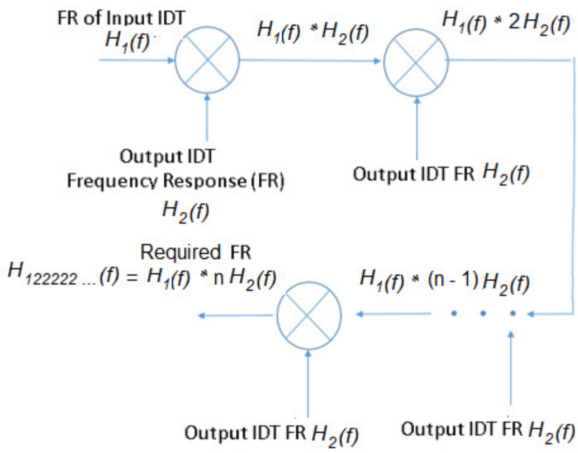

Fig. 10: General cascaded frequency-response structure used to obtain $H_{c,K}(f)$.

4.3 Generalized Cascade Formulation

The iterative process can be written in recursive form as

$$H_{c,K}(f) = H_{c,K-1}(f) H_{out}(f), \qquad K \geq 2, \tag{20}$$

with the initial condition

$$H_{c,1}(f) = H_{in}(f) H_{out}(f). \tag{21}$$

Using this recursive definition, the response after K output-response applications is

$$H_{c,K}(f) = H_{in}(f) \left[H_{out}(f)\right]^{K}. \tag{22}$$

Here, $H_{c,K}(f)$ denotes the Kth cascaded composite response. Thus, $K = 1$ corresponds to the baseline response, $K = 2$ corresponds to the second-order cascaded response, and $K = 3$ corresponds to the third-order cascaded response.

Figure 10 presents the general block representation of the proposed methodology. From a system-analysis point of view, (22) shows that the output transducer acts as the principal repeated weighting function in the cascade. Therefore, the proposed approach can be interpreted as a spectral sharpening mechanism based on repeated response shaping by the output IDT.

4.4 Performance-Parameter Extraction

For each cascade order, the resulting composite response is evaluated using four performance parameters that are commonly employed in SAW-filter characterization [6–8]:

- **Center frequency**: the frequency at which the main-lobe peak occurs.
- Peak response level and insertion-loss magnitude: the peak magnitude level $G_{p,K}$ is reported in decibels, while the corresponding insertion-loss magnitude is defined as $IL_K = -G_{p,K}$.
- **Side-lobe rejection**: the difference, in decibels, between the main-lobe peak and the largest side-lobe level.
- **3-dB bandwidth**: the frequency span between the two frequencies at which the response falls by 3 dB from the main-lobe peak.

These four metrics are extracted for every cascade order in order to quantify the effect of repeated response multiplication. The center frequency is used to track any passband shift, the insertion loss indicates the attenuation penalty associated with repeated cascading, the side-lobe rejection measures the improvement in out-of-band suppression, and the 3-dB bandwidth reflects the sharpening of the passband. Together, these parameters provide a complete description of the selectivity–loss trade-off introduced by the proposed methodology.

In summary, the proposed cascaded frequency-response method consists of three main steps: first, the individual IDT responses are computed using the delta-function model; second, a baseline two-port SAW-filter response is obtained; and third, the output-IDT response is repeatedly multiplied with the composite response to generate higher-order cascaded responses. This procedure enables a systematic study of how repeated spectral shaping influences the main filtering characteristics of a uniformly apodized SAW filter.

5 Simulation Setup and Performance Metrics

The frequency responses of the uniformly apodized SAW filter were simulated numerically in MATLAB [20]. The input- and output-IDT responses were first calculated using the delta-function model described in Section 2. The baseline two-port response was then obtained from the product of the input- and output-IDT responses, and the higher-order cascaded responses were generated by repeated multiplication with the output-IDT response. This procedure follows the frequency-domain representation of linear SAW transversal filters, in which the overall magnitude response is governed by the combined responses of the IDTs and the acoustic propagation path [6–8, 13].

For a cascade order K, the simulated response is expressed as

$$H_{c,K}(f) = H_{in}(f)\,[H_{out}(f)]^K\,, \qquad K = 1,2,\ldots,50. \quad (23)$$

where $H_{in}(f)$ and $H_{out}(f)$ are the input- and output-IDT frequency responses, respectively. In this notation, $K = 1$ corresponds to the baseline response $H_{c,1}(f) = H_{in}(f)H_{out}(f)$, $K = 2$ corresponds to $H_{c,2}(f) = H_{in}(f)[H_{out}(f)]^2$, and $K = 3$ corresponds to $H_{c,3}(f) = H_{in}(f)[H_{out}(f)]^3$.

The main simulation set was performed for cascade orders from $K = 1$ to $K = 50$. Additional high-order cases were also evaluated at $K = 1000$, 5000, 10000, 100000, 500000, and 1000000 in order to illustrate the model-predicted narrowband and ultra-narrowband trends. These high-order cases should be interpreted as ideal frequency-response predictions obtained from repeated response multiplication, rather than as direct experimental performance limits of a practical fabricated SAW device.

A fixed triple-transit-interference loss term may be included as a scalar amplitude correction in the simulated transfer response [19]. Since this term is frequency independent, it changes the absolute response level but does not affect the extracted center frequency, side-lobe rejection, or 3-dB bandwidth. Other second-order effects, such as electromagnetic feedthrough, electrode reflections, diffraction, impedance mismatch, and propagation loss, are not explicitly included in the present simulation model.

For each cascade order, four performance metrics were extracted: center frequency, peak response level, side-lobe rejection, and 3-dB bandwidth. These quantities are commonly used to characterize the frequency-selective behavior of SAW filters [6–8]. The extraction procedure is described below.

5.1 Center Frequency

The center frequency is defined as the frequency at which the main-lobe magnitude reaches its maximum value. For the Kth cascaded response, it is calculated as

$$f_{c,K} = \arg\max_f |H_{c,K}(f)| \quad (24)$$

The corresponding peak magnitude in decibels is

$$G_{p,K} = 20\log_{10}|H_{c,K}(f_{c,K})| \quad (25)$$

5.2 Insertion-Loss Convention

In this paper, the simulated peak response level is reported in decibels using (25). Since the magnitude of the transfer response is less than unity, $G_{p,K}$ is negative. The insertion-loss magnitude can therefore be written as

$$\mathrm{IL}_K = -20\log_{10}|H_{c,K}(f_{c,K})| \quad (26)$$

Thus, a reported peak level of -11.31 dB corresponds to an insertion-loss magnitude of 11.31 dB. This convention avoids ambiguity between the negative response level and the positive insertion-loss quantity.

5.3 Side-Lobe Rejection

The side-lobe rejection is calculated from the difference between the main-lobe peak level and the largest side-lobe level. Let $f_{sl,K}$ denote the frequency at which the largest side lobe occurs outside the main-lobe region. The side-lobe rejection is then given by

$$\mathrm{SLR}_K = G_{p,K} - 20\log_{10}\left|H_{c,K}(f_{sl,K})\right|. \quad (27)$$

A larger value of SLR_K indicates stronger suppression of the largest side lobe relative to the main response peak.

5.4 3-dB Bandwidth

The 3-dB bandwidth is defined as the frequency interval between the lower and upper frequencies at which the response level falls by 3 dB from the main-lobe peak. These frequencies satisfy

$$20\log_{10}|H_{c,K}(f_{L,K})| = G_{p,K} - 3, \quad (28)$$

and

$$20\log_{10}|H_{c,K}(f_{H,K})| = G_{p,K} - 3. \quad (29)$$

The 3-dB bandwidth is therefore

$$\mathrm{BW}_{3dB,K} = f_{H,K} - f_{L,K}. \quad (30)$$

This metric is used to quantify the passband sharpening produced by the proposed cascaded frequency-response method.

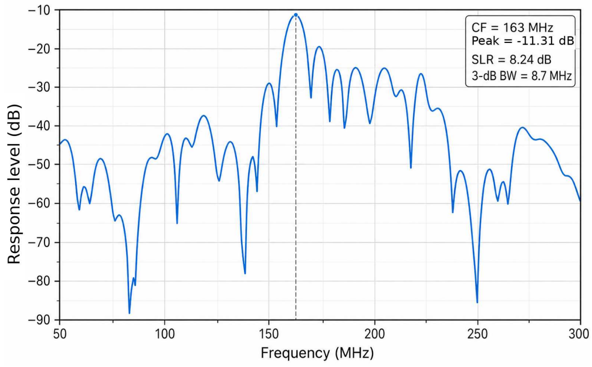

Fig. 11: Frequency response of the baseline SAW filter, $H_{c,1}(f) = H_{in}(f)H_{out}(f)$.

6 Simulated Frequency-Response Results

6.1 Baseline and Low-Order Cascaded Responses

Figure 11 shows the baseline response, denoted here as $H_{c,1}(f)$ and labeled in the figure as $H_{12}(f)$. This response corresponds to

$$H_{c,1}(f) = H_{in}(f)H_{out}(f). \tag{31}$$

and represents the first cascade order, $K = 1$. The extracted center frequency is approximately 163 MHz. The peak response level is -11.31 dB, corresponding to an insertion-loss magnitude of 11.31 dB. The side-lobe rejection is 8.24 dB, and the 3-dB bandwidth is approximately 8.70 MHz.

The second-order cascaded response is obtained by multiplying the baseline response by the output-IDT response:

$$H_{c,2}(f) = H_{c,1}(f)H_{out}(f) = H_{in}(f)\left[H_{out}(f)\right]^2. \tag{32}$$

As shown in Fig. 12, the main passband becomes narrower and the side lobes are further suppressed. The center frequency shifts to approximately 162 MHz, the peak response level decreases to -17.43 dB, the side-lobe rejection increases to 19.70 dB, and the 3-dB bandwidth decreases to 5.04 MHz.

The third-order response is calculated as

$$H_{c,3}(f) = H_{c,2}(f)H_{out}(f) = H_{in}(f)\left[H_{out}(f)\right]^3. \tag{33}$$

Figure 13 shows that the selectivity improvement continues with increasing cascade order. The center frequency remains approximately 162 MHz, while the peak response level decreases to -23.43 dB. The side-lobe rejection increases to 31.29 dB, and the 3-dB bandwidth decreases to 4.13 MHz.

These low-order results confirm the expected behavior of the proposed method: repeated multiplication by the output-IDT response suppresses frequency components away from the main lobe, thereby increasing side-lobe rejection and reducing the 3-dB bandwidth. However, this improvement comes at the cost of a lower peak response level, resulting in a larger insertion loss magnitude.

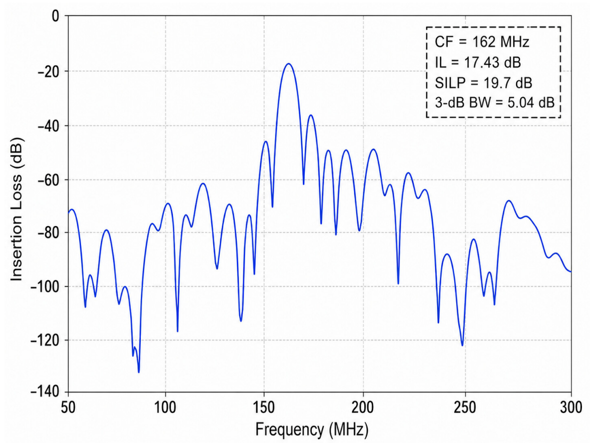

Fig. 12: Frequency response of the second-order cascaded response, $H_{122}(f)$.

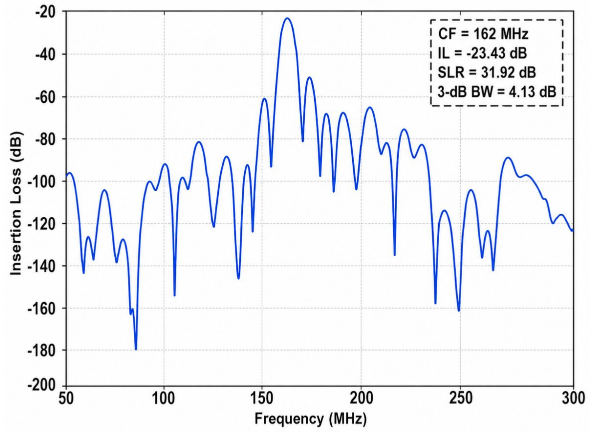

Fig. 13: Frequency response of the third-order cascaded response, $H_{1222}(f)$.

6.2 Results up to 50 Cascades

Table 3 summarizes the extracted frequency-response parameters for cascade orders from $K = 1$ to $K = 50$. The center frequency remains approximately constant at 162 MHz after the first cascade order. In contrast, the peak response level decreases almost uniformly as the cascade order increases, indicating a progressive insertion-loss penalty. Over the same range, the side-lobe rejection increases from 8.24 dB to 575.80 dB, while the 3-dB bandwidth decreases from 8.70 MHz to 0.549 MHz.

Table 3: Frequency-response parameters of the uniformly apodized SAW filter for cascade orders from $K = 1$ to $K = 50$.

Cascade order K	center frequency (MHz)	Peak response level $G_{p,K}$ (dB)	side-lobe rejection (dB)	3-dB bandwidth (MHz)
1	163	-11.31	8.24	8.700
2	162	-17.43	19.70	5.040
3	162	-23.43	31.29	4.130
4	162	-29.44	42.88	3.550
5	162	-35.43	54.46	3.100
6	162	-41.44	66.06	2.810
7	162	-47.44	77.66	2.610
8	162	-53.44	89.16	2.440
9	162	-59.44	100.76	2.326
10	162	-65.45	112.34	2.230
11	162	-71.45	123.96	2.148
12	162	-77.45	135.56	2.082
13	162	-83.45	147.16	2.029
14	162	-89.45	158.75	1.928
15	162	-95.45	170.26	1.797
16	162	-101.50	181.80	1.685
17	162	-107.45	193.45	1.590
18	162	-113.45	205.05	1.505
19	162	-119.45	216.65	1.425
20	162	-125.50	228.20	1.355
21	162	-131.46	239.84	1.293
22	162	-137.46	251.34	1.234
23	162	-143.46	262.94	1.180
24	162	-149.46	274.54	1.128
25	162	-155.46	286.13	1.0865
26	162	-161.47	297.73	1.048
27	162	-167.47	309.33	1.009
28	162	-173.47	320.93	0.973
29	162	-179.48	332.42	0.940
30	162	-185.50	343.80	0.910
31	162	-191.48	355.62	0.881
32	162	-197.48	367.22	0.854
33	162	-203.48	378.82	0.827
34	162	-209.48	390.42	0.803
35	162	-215.48	402.02	0.780
36	162	-221.48	413.52	0.759
37	162	-227.48	425.12	0.738
38	162	-233.50	436.70	0.718
39	162	-239.49	448.31	0.701
40	162	-245.50	459.91	0.685
41	162	-251.50	471.50	0.670
42	162	-257.49	483.11	0.652
43	162	-263.49	494.71	0.636
44	162	-269.49	506.21	0.622
45	162	-275.50	517.80	0.611
46	162	-281.50	529.40	0.5965
47	162	-287.50	541.00	0.584
48	162	-293.50	552.60	0.571
49	162	-299.50	564.20	0.561
50	162	-305.50	575.80	0.549

The results in Table 3 show two main trends. First, the side-lobe rejection increases strongly with cascade order because each additional multiplication by $H_{\text{out}}(f)$ further attenuates the side-lobe regions. Second, the 3-dB bandwidth decreases monotonically because the effective passband becomes increasingly concentrated around the main-lobe peak. The decrease in peak response level is the main limitation of the proposed approach, since higher cascade orders provide stronger selectivity but also produce a larger attenuation penalty.

6.3 Dynamic-Range-Limited Interpretation of Side-Lobe Rejection

The side-lobe-rejection values in Table 3 and Table 4 are relative values obtained from the ideal simulated magnitude response. They should not be interpreted as directly measurable rejection levels without considering the available dynamic range. In practice, the measurable rejection is limited by the instrument noise floor, electromagnetic feedthrough, substrate-related parasitic responses, impedance mismatch, and numerical or measurement dynamic range. Therefore, once the peak response level becomes very small, additional mathematical rejection may no longer translate into observable device-level rejection.

For this reason, the practically useful cascade range should be selected using both the target side-lobe rejection and the allowable insertion-loss budget. Low and moderate cascade orders may provide useful selectivity improvement, whereas very high cascade orders mainly illustrate the ideal mathematical trend of the response-synthesis process. The high rejection values

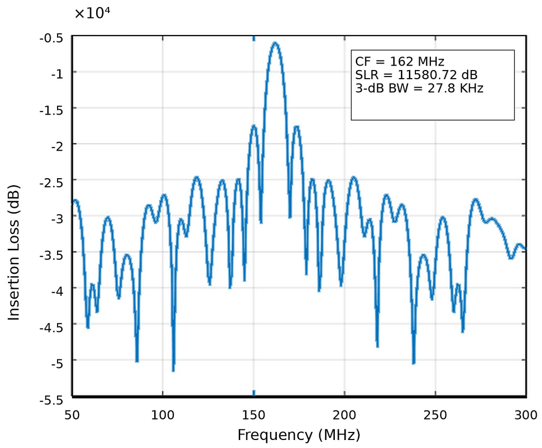

Fig. 14: Model-predicted frequency response for $K = 1000$ cascaded iterations.

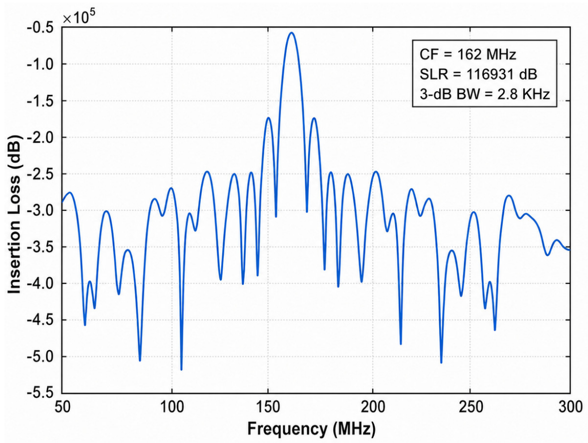

Fig. 15: Model-predicted frequency response for $K = 10000$ cascaded iterations.

predicted at large K should therefore be treated as upper-bound model indicators rather than practical rejection specifications.

Table 4 shows that the most relevant engineering result is not the maximum theoretical side-lobe rejection, but the trade-off between rejection, bandwidth, and peak response level. Therefore, a practical design should choose K from the lowest order that satisfies the required side-lobe rejection and bandwidth while keeping the peak response above the system noise and dynamic-range limits.

6.4 High-Order Narrowband and Ultra-Narrowband Responses

To investigate the asymptotic behavior of the cascaded response, additional high-order simulations were performed. Figures 14–16 show the simulated responses for $K = 1000$, 10000, and 1000000. These cases are included to illustrate the theoretical narrowing trend predicted by the ideal delta-function model.

The extracted parameters for these high-order cases are summarized in Table 5. The center frequency remains approximately fixed at 162 MHz. The predicted 3-dB bandwidth decreases from 27.8 kHz at $K = 1000$ to 12.5 Hz at $K = 1000000$. The corresponding side-lobe-rejection values become extremely large because the model repeatedly multiplies the response in the linear domain and then converts the result to decibels.

The high-order responses demonstrate the mathematical capability of the proposed cascaded frequency-response method to produce very narrow passbands in the ideal model. However, these results should not be interpreted as directly achievable measured rejection levels in a practical SAW device. At very large cascade orders, the response level becomes extremely

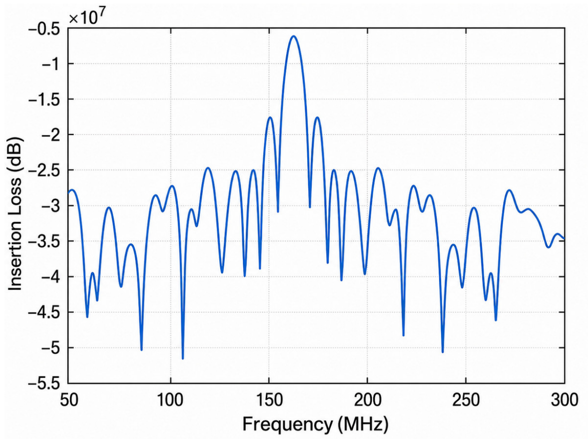

Fig. 16: Model-predicted frequency response for $K = 1000000$ cascaded iterations.

small, and practical effects such as propagation loss, electrode reflections, impedance mismatch, electromagnetic feedthrough, diffraction, fabrication tolerance, and noise floor limitations would strongly affect the measurable response. Therefore, the high-order cases are most useful as trend indicators for narrowband and ultra-narrowband response synthesis rather than as direct physical implementation targets.

Overall, the simulated results confirm that increasing the cascade order improves side-lobe rejection and sharpens the 3-dB bandwidth, while simultaneously increasing the insertion-loss magnitude. This selectivity–loss trade-off motivates the regression analysis presented in the next section, where compact predictive equations are developed for side-lobe rejection and 3-dB bandwidth as functions of cascade order.

Table 4: Dynamic-range-limited interpretation of side-lobe rejection for selected cascade orders.

Effective cascade order K	side-lobe rejection (dB)	3-dB bandwidth	Peak response level (dB)	Practical interpretation
1	8.24	8.70 MHz	-11.31	Baseline response
5	54.46	3.10 MHz	-35.43	Potentially useful if loss budget allows
10	112.34	2.23 MHz	-65.45	Requires careful gain/noise planning
20	228.20	1.355 MHz	-125.50	Mostly theoretical for passive implementation
50	575.80	0.549 MHz	-305.50	Ideal mathematical trend only

Table 5: Model-predicted frequency-response parameters for high-order narrowband and ultra-narrowband cases.

Cascade order K	center frequency (MHz)	side-lobe rejection (dB)	3-dB bandwidth
1000	162	11580.72	27.8 kHz
5000	162	57917	5.6 kHz
10000	162	116931	2.8 kHz
100000	162	1158420	275.5 Hz
500000	162	5792090	55.2 Hz
1000000	162	11584150	12.5 Hz

7 Regression Modeling and Performance Prediction

The simulated results in Section 6 show that increasing the effective frequency-response cascade order produces two dominant trends: the side-lobe rejection increases strongly, whereas the 3-dB bandwidth decreases monotonically. To express these trends in compact mathematical form, empirical regression models are developed for side-lobe rejection and 3-dB bandwidth as functions of cascade order. These models are intended for rapid preliminary estimation and design screening, rather than as universal physical laws for SAW-filter behavior.

Unless otherwise stated, all regression equations in this section are calibrated using the simulated data for $1 \leq K \leq 50$. Therefore, the fitted equations should be interpreted as interpolation models within this range. Their use for $K > 50$ should be treated only as trend extrapolation and not as validated design prediction. This restriction is important because high cascade orders are affected by insertion-loss accumulation, numerical dynamic range, noise-floor limits, fabrication tolerance, impedance mismatch, and second-order acoustic effects that are not fully represented in the present delta-function model. Regression modeling remains useful in this context because it provides closed-form expressions for rapid performance estimation without repeating the full frequency-response simulation for every candidate cascade order [21–24].

7.1 Linear Model for Side-Lobe Rejection

Over the calibrated range $1 \leq K \leq 50$, the side-lobe rejection exhibits a nearly linear dependence on the effective frequency-response cascade order. This behavior is expected from the logarithmic representation of the response magnitude. Since each additional cascade multiplies the composite response by the same output-IDT response, the relative attenuation of the side-lobe region increases by an approximately constant amount when expressed in decibels.

Table 6: Representative side-lobe-rejection data used for linear regression.

Cascade order K	side-lobe rejection (dB)
1	8.24
2	19.70
3	31.29
4	42.88
5	54.46
10	112.34
20	228.20
30	343.80
40	459.91
50	575.80

The side-lobe-rejection data used for the linear fit are summarized in Table 6. The fitted linear model is

$$\mathrm{SLR}(K) = 11.58K - 3.469, \tag{34}$$

where $\mathrm{SLR}(K)$ is the predicted side-lobe rejection in decibels and K is the cascade order. The slope of (34) indicates that each additional cascade contributes approximately 11.58 dB of side-lobe-rejection improvement within the simulated range.

This equation is calibrated for the simulated rectangular-window SAW response and should not be interpreted as a universal side-lobe-rejection law for all SAW-filter geometries.

The quality of the linear fit is shown in Fig. 17. The fitted model gives a coefficient of determination of approximately

$$R^2 \approx 0.999999999, \tag{35}$$

and a root-mean-square error of

$$\mathrm{RMSE} = 0.051687\ \mathrm{dB}. \tag{36}$$

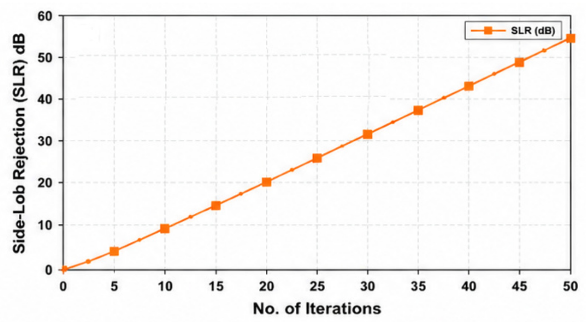

Fig. 17: Linear relationship between cascade order and side-lobe rejection.

Table 7: Representative 3-dB bandwidth values used for nonlinear regression.

Cascade order K	3-dB bandwidth (MHz)
1	8.700
2	5.040
3	4.130
4	3.550
5	3.100
10	2.230
20	1.355
30	0.910
40	0.685
50	0.549

These values indicate that the linear model provides an excellent empirical fit to the simulated side-lobe-rejection data over $1 \leq K \leq 50$, consistent with standard regression accuracy measures used in engineering analysis [25]. The small RMSE supports the use of (34) as a compact interpolation equation within the fitted range. However, extrapolation to much larger cascade orders should be interpreted only as a mathematical trend and not as a validated physical prediction.

For design purposes, (34) can also be rearranged to estimate the cascade order required to achieve a target side-lobe rejection:

$$K_{\mathrm{SLR}} = \frac{\mathrm{SLR}_{\mathrm{target}} + 3.469}{11.58}. \tag{37}$$

Since K must be an integer in the cascaded-response procedure, the calculated value from (37) should be rounded up to the nearest integer when a minimum target rejection must be satisfied.

Equation (37) is useful for estimating the minimum cascade order required to reach a target side-lobe rejection within the calibrated range. For targets that lead to $K > 50$, the result should be considered an extrapolated estimate. In such cases, the predicted cascade order must also be checked against the allowable peak-response level, insertion-loss budget, and measurement dynamic range.

The extracted side-lobe-rejection regression model provides a direct design-estimation relationship between cascade order and SLR. Using the fitted linear equation, the expected side-lobe rejection can be estimated from a specified number of cascades, and the required cascade order can also be calculated for a target SLR value. This makes the regression model useful as a compact analytical tool for early-stage SAW-filter design assessment.

7.2 Nonlinear Modeling of 3-dB Bandwidth

Unlike the side-lobe rejection, the 3-dB bandwidth does not follow a linear trend. The bandwidth decreases rapidly during the first few cascades and then decreases more gradually as the cascade order increases. This nonlinear behavior occurs because repeated multiplication by the output-IDT response progressively concentrates the composite response around the main-lobe peak, but the rate of bandwidth reduction diminishes at higher cascade orders.

Representative bandwidth values are listed in Table 7. The complete data set corresponds to the 50 cascade orders reported in Table 3. Three nonlinear models were evaluated: an eight-term Gaussian model, a tenth-degree polynomial model, and a two-term power-law model. The Gaussian model provides the most accurate fit, the polynomial model provides an alternative high-order approximation, and the power-law model provides the simplest closed-form expression for practical design estimation.

7.2.1 Eight-Term Gaussian Model

Among the tested empirical models, the eight-term Gaussian model produced the lowest fitting error over the calibrated range $1 \leq K \leq 50$, consistent with the use of Gaussian models for frequency-response data fitting [26]. This model can represent the strongly nonlinear bandwidth contraction over the simulated interval and is expressed as

$$y(K) = \sum_{i=1}^{8} a_i \exp\left[-\left(\frac{x-b_i}{c_i}\right)^2\right], \tag{38}$$

where $y(K)$ is the predicted 3-dB bandwidth in megahertz and x is the standardized cascade order. The standardized variable is defined as

$$x = \frac{K-\mu_K}{\sigma_K}, \tag{39}$$

with

$$\mu_K = 25.5, \qquad \sigma_K = 14.58. \tag{40}$$

Table 8: Coefficients of the eight-term Gaussian model for 3-dB bandwidth fitting.

Term i	a_i	b_i	c_i
1	15090	-2.335	0.2297
2	1.687	-1.614	0.1984
3	0.2677	-1.304	0.1364
4	0.1702	-1.099	0.1439
5	0.1432	-0.8605	0.1453
6	0.1074	-0.7573	0.3113
7	0.9261	-2.379	5.535
8	2.182	-2.517	1.784

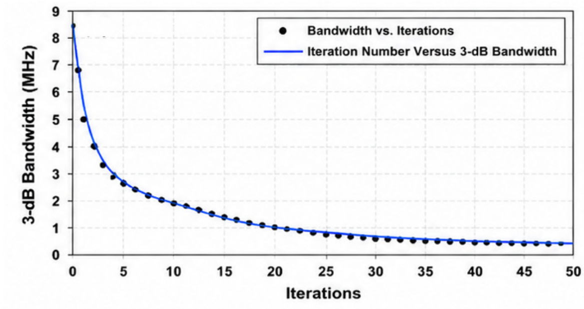

Fig. 18: Eight-term Gaussian fit for the 3-dB bandwidth versus cascade order.

The fitted Gaussian coefficients are listed in Table 8. This model produced a sum of squared errors of

$$\mathrm{SSE} = 1.306 \times 10^{-4}, \tag{41}$$

a coefficient of determination that is approximately unity over the fitted numerical data,

$$R^2 \approx 1, \tag{42}$$

and a root-mean-square error of

$$\mathrm{RMSE} = 0.002242 \text{ MHz}. \tag{43}$$

These values show that the Gaussian model closely reproduces the simulated bandwidth values within the fitted data set. However, the near-unity value of R^2 should not be interpreted as physical validation of the model. The Gaussian expression is a high-parameter empirical interpolation function, and its accuracy is demonstrated only for the simulated data over $1 \leq K \leq 50$. It should therefore be used for interpolation within this range, not for extrapolating high-order narrowband or ultra-narrowband behavior.

7.2.2 Tenth-Degree Polynomial Model

A tenth-degree polynomial model was also fitted to the bandwidth data, following the common use of high-order polynomial regression for RF-filter parameter

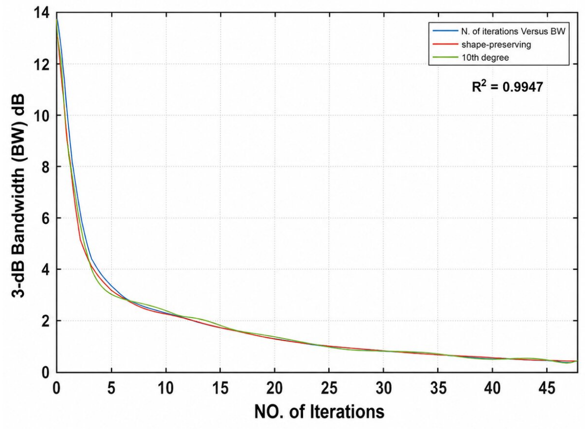

Fig. 19: Tenth-degree polynomial fit for the 3-dB bandwidth versus cascade order.

extraction [27]. The polynomial model is included only as a descriptive numerical fit and not as the preferred design equation, because high-degree polynomials can behave poorly near the boundaries of the fitted interval and can give unrealistic values outside the calibration range. The polynomial model is given by

$$\begin{aligned} y(K) = {} & 6.446 \times 10^{-13} K^{10} - 1.74 \times 10^{-10} K^9 + 2.03 \times 10^{-8} K^8 \\ & - 1.341 \times 10^{-6} K^7 + 5.521 \times 10^{-5} K^6 - 0.00147 K^5 \\ & + 0.02544 K^4 - 0.2803 K^3 + 1.87 K^2 - 6.924 K + 13.8. \end{aligned} \tag{44}$$

Here, $y(K)$ is the predicted 3-dB bandwidth in megahertz and K is the cascade order.

The polynomial fit gives

$$R^2 = 0.9947, \tag{45}$$

which indicates that the model explains approximately 99.47% of the variance in the simulated bandwidth data. However, high-degree polynomial models can be sensitive near the boundaries of the fitted interval and may produce unrealistic behavior when extrapolated outside the calibration range [21, 22]. Therefore, (44) should be used only to describe the simulated data over $1 \leq K \leq 50$. It should not be used to predict bandwidth for high cascade orders or to support ultra-narrowband design claims.

7.2.3 Two-Term Power-Law Model

For practical design use, a simpler two-term power-law model was fitted to the bandwidth data using the two-term power-fit form available in MATLAB curve fitting tools [28]. The general form of the model is

$$y(K) = aK^b + c, \tag{46}$$

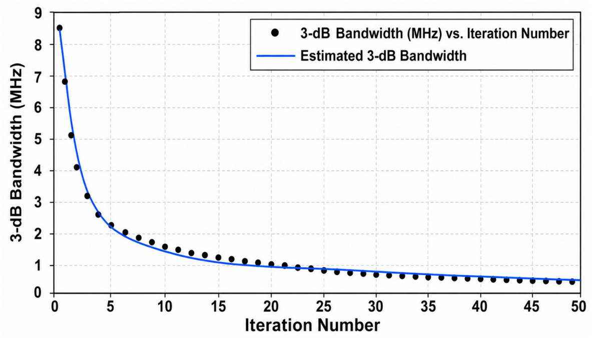

Fig. 20: Two-term power-law fit for the 3-dB bandwidth versus cascade order.

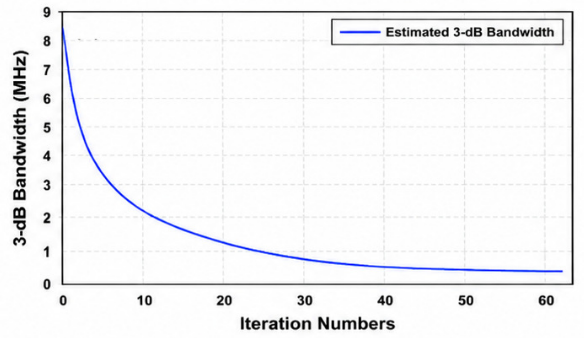

Fig. 21: MATLAB prediction of 3-dB bandwidth using the two-term power-law model.

where $y(K)$ is the 3-dB bandwidth in megahertz and K is the cascade order. The fitted coefficients are

$$a = 8.809, \qquad b = -0.5349, \qquad c = -0.4827. \tag{47}$$

Therefore, the final power-law bandwidth model is

$$\mathrm{BW}_{3\mathrm{dB}}(K) = 8.809K^{-0.5349} - 0.4827. \tag{48}$$

This expression is recommended only for preliminary estimation over the calibrated range $1 \leq K \leq 50$. Its simplicity makes it useful for engineering interpretation, but it is less accurate than the Gaussian interpolation model and should not be used as a validated predictor for very high cascade orders.

The two-term power-law model gives

$$R^2 = 0.9896, \qquad \mathrm{SSE} = 1.03, \qquad \mathrm{RMSE} = 0.1481\,\mathrm{MHz}. \tag{49}$$

Although this model is less accurate than the Gaussian and tenth-degree polynomial fits, it has a much simpler structure and is easier to use in preliminary filter design. It also captures the dominant nonlinear trend of bandwidth reduction with increasing cascade order.

Solving (46) for K gives an inverse relation that can be used to estimate the required cascade order for a target 3-dB bandwidth. Starting from

$$y - c = aK^b, \tag{50}$$

and taking the natural logarithm of both sides gives

$$\ln(y - c) = \ln(a) + b\ln(K). \tag{51}$$

Thus,

$$\ln(K) = \frac{\ln(y - c) - \ln(a)}{b}, \tag{52}$$

and the required cascade order is

$$K = \exp\left[\frac{\ln(y - c) - \ln(a)}{b}\right]. \tag{53}$$

Substituting the fitted coefficients gives

$$K = \exp\left[\frac{\ln(y + 0.4827) - \ln(8.809)}{-0.5349}\right]. \tag{54}$$

When the inverse equation gives $K > 50$, the result should be interpreted as an extrapolated indication of the required cascade order. It should not be used alone to claim practical bandwidth realization unless the corresponding insertion loss, noise floor, and dynamic-range limits are also evaluated.

In (54), y is the desired 3-dB bandwidth in megahertz. Since the cascade order must be an integer, the value predicted by (54) should be rounded to the nearest practical integer, or rounded upward when the design must not exceed a specified bandwidth. This inverse equation is useful for early-stage estimation of the number of response cascades required to approach a target bandwidth.

Figure 21 shows the MATLAB implementation of the power-law prediction model. The inverse bandwidth-estimation model provides a rapid design-screening tool for either estimating the 3-dB bandwidth from a specified cascade order or determining the required cascade order from a target bandwidth. Using the fitted power-series relationship, the designer can directly evaluate the trade-off between cascade order and bandwidth reduction without repeating the full frequency-response simulation.

7.3 Comparison of the Regression Models

The three bandwidth models provide different trade-offs between accuracy and simplicity. The eight-term Gaussian model gives the best numerical fit, with an RMSE of only 0.002242 MHz, but it requires 24 fitting coefficients and a standardized input variable. The tenth-degree polynomial model is less complex than the Gaussian model but is still relatively high order and may be sensitive when used outside the fitted interval. The two-term power-law model has the lowest fitting accuracy among the three models, but it is the most compact and provides a direct inverse expression for estimating the cascade order required to satisfy a target bandwidth.

For this reason, the Gaussian model is recommended when accurate interpolation over $1 \le K \le 50$ is required, whereas the power-law model is more suitable for rapid design estimation and graphical-interface implementation using tools such as LabVIEW [29, 30]. The polynomial model provides an intermediate descriptive fit but is not the preferred model for extrapolation.

Overall, the regression analysis confirms two predictable trends within the simulated range $1 \le K \le 50$. First, the side-lobe rejection increases nearly linearly with cascade order. Second, the 3-dB bandwidth decreases nonlinearly and can be approximated using empirical bandwidth models. These equations are useful for early-stage design screening because they provide rapid estimates of the selectivity–loss trade-off. However, they are calibrated to the present rectangular-window SAW geometry and the ideal delta-function simulation framework. Therefore, predictions outside the fitted range should be treated as trend extrapolations and should be verified using higher-fidelity acoustic modeling or experimental measurements. Table 9 summarizes the recommended use of each regression model. The Gaussian model is most appropriate when accurate interpolation of the simulated data is required, whereas the two-term power-law model is more convenient for preliminary design calculations. None of the regression models should be used as a standalone predictor for very high cascade orders without additional loss, noise-floor, and physical-device modeling.

8 Discussion

The simulated results demonstrate that the proposed cascaded frequency-response method provides a systematic way to improve the selectivity of a uniformly apodized SAW filter. The central mechanism is the repeated multiplication of the composite response by the output-IDT response. Since the output-IDT response has its maximum value near the main passband and lower magnitude in the side-lobe regions, each additional cascade suppresses the off-peak spectral components more strongly than the main-lobe component. This behavior is consistent with the frequency-domain interpretation of transversal SAW filters, where the overall filter response is governed by the product of the individual IDT responses and the acoustic propagation term [6–8].

A key observation is that the center frequency remains nearly constant after the first cascade order. The baseline response $H_{c,1}(f)$, also denoted as $H_{12}(f)$ in the figures, has a center frequency of approximately 163 MHz, whereas the cascaded responses from $K = 2$ to $K = 50$ remain close to 162 MHz. This indicates that the repeated multiplication process primarily modifies the shape of the magnitude response rather than shifting the passband. The stability of the center frequency is important because it suggests that the proposed method can improve selectivity while preserving the intended operating frequency of the output-IDT-dominated response.

The side-lobe rejection increases almost linearly with cascade order. This trend can be explained by the logarithmic decibel representation of the response. In the linear magnitude domain, each cascade multiplies the existing response by the same output-IDT response. In the decibel domain, this repeated multiplication becomes an approximately additive process. Therefore, each additional cascade contributes nearly the same rejection increment between the main-lobe peak and the largest side lobe. This explains the fitted linear relation

$$\mathrm{SLR}(K) = 11.58K - 3.469, \tag{55}$$

which accurately represents the simulated side-lobe-rejection trend over the fitted range $1 \le K \le 50$.

In contrast, the 3-dB bandwidth decreases nonlinearly with increasing cascade order. The most rapid reduction occurs during the first few cascades, where the bandwidth decreases from 8.70 MHz at $K = 1$ to 5.04 MHz at $K = 2$ and 4.13 MHz at $K = 3$. At higher cascade orders, the rate of reduction becomes more gradual, reaching 0.549 MHz at $K = 50$. This nonlinear behavior reflects the progressive concentration of the response around the main-lobe peak. As the response becomes increasingly narrow, additional cascades still sharpen the passband, but the incremental bandwidth reduction becomes smaller.

The improvement in selectivity is accompanied by a significant reduction in peak response level. This is the principal practical limitation of the proposed approach. For the baseline response, the peak response level is approximately -11.31 dB. After 50 cascades, it decreases to approximately -305.50 dB. In insertion-loss terms, this corresponds to a very large attenuation penalty. Therefore, the method produces a clear selectivity–loss trade-off: higher cascade orders provide stronger side-lobe suppression and narrower 3-dB bandwidth, but they also lead to much lower output amplitude.

This trade-off must be considered carefully when interpreting the results. Low and moderate cascade orders may be useful for improving side-lobe rejection and bandwidth selectivity while keeping the attenuation within a more manageable range. Very high cascade orders, on the other hand, produce extremely sharp model-predicted responses but also extremely small output levels. In a practical implementation, this would require careful consideration of source and load impedance, matching networks, amplification, dynamic range, thermal noise, substrate loss, and fabrication tolerance. Such effects are known to influence practical SAW-filter behavior and are not fully represented by the simplified delta-function model [6–8, 13].

The regression models extracted in Section 7 provide useful early-stage design tools. The linear

Table 9: Recommended use and validity range of the regression models.

Model	Intended use	Validated/calibrated range	Recommended for extrapolation?	Comment
Linear side-lobe rejection model	Fast estimation of side-lobe rejection	$1 \leq K \leq 50$	No	Excellent empirical fit within the fitted range
Eight-term Gaussian bandwidth model	Accurate interpolation of 3-dB bandwidth	$1 \leq K \leq 50$	No	Highest numerical fit, but many parameters
Tenth-degree polynomial bandwidth model	Descriptive curve fit	$1 \leq K \leq 50$	No	Possible boundary oscillation and overfitting
Two-term power-law bandwidth model	Simple design estimation and inverse calculation	$1 \leq K \leq 50$	Limited trend only	Useful for preliminary estimates, not high-order validation

side-lobe-rejection model gives a direct estimate of the cascade order required to achieve a target rejection level. Similarly, the power-law bandwidth model provides a compact approximation for estimating the cascade order required to approach a desired 3-dB bandwidth. These models are especially useful during preliminary design because they reduce the need to repeat the full frequency-response simulation for each candidate cascade order. However, the models should be treated as empirical predictors calibrated to the simulated rectangular-window structure over $1 \leq K \leq 50$. Their use at larger cascade orders should be regarded as trend extrapolation and must be interpreted together with insertion-loss, noise-floor, dynamic-range, and second-order acoustic limitations.

Among the bandwidth models, the eight-term Gaussian model provides the highest fitting accuracy over the simulated range, but it is mathematically complex and contains many fitting parameters. The tenth-degree polynomial model also provides a strong fit but may be sensitive near the boundaries of the fitted interval and is not preferred for extrapolation. The two-term power-law model is less accurate than the Gaussian model but is more convenient for engineering use because it has a simple closed form and can be inverted to estimate the required cascade order from a target bandwidth. Therefore, the Gaussian model is most suitable for accurate interpolation, while the power-law model is more suitable for rapid design estimation.

It is important to emphasize that the proposed method should be interpreted as a frequency-response synthesis and analysis approach rather than as a direct physical layout of many cascaded SAW devices. The repeated multiplication process shows how the response evolves when the output-IDT spectral weighting is applied multiple times. This provides valuable insight into the relationship between cascade order, side-lobe suppression, bandwidth sharpening, and attenuation. A practical device implementation would require additional design considerations, including physical cascading, impedance matching, acoustic loss, electrode reflections, electromagnetic feedthrough, and possible amplification or compensation stages.

Overall, the discussion confirms that the proposed cascaded frequency-response method is effective for studying selectivity enhancement in SAW filters. The main advantage of the method is its ability to generate predictable improvements in side-lobe rejection and 3-dB bandwidth using a simple response-multiplication framework. The main limitation is the associated insertion-loss increase, which becomes severe at high cascade orders. Therefore, practical use of the method requires selecting a cascade order that balances the required side-lobe rejection and bandwidth against the allowable loss budget.

9 Narrowband and Ultra-Narrowband Implications

The high-order simulations indicate that the proposed cascaded frequency-response method can theoretically generate very narrow 3-dB bandwidths. In the ideal model, the bandwidth decreases from 27.8 kHz at $K = 1000$ to 5.6 kHz at $K = 5000$ and 2.8 kHz at $K = 10000$. For still higher cascade orders, the model predicts bandwidths of 275.5 Hz at $K = 100000$, 55.2 Hz at $K = 500000$, and 12.5 Hz at $K = 1000000$. These results demonstrate the mathematical narrowing trend produced by repeated response multiplication.

These high-order cases are not obtained from the regression models calibrated in Section VII; they are direct ideal response-multiplication simulations and should be interpreted separately from the $1 \leq K \leq 50$ empirical fits.

Such narrowband behavior may be relevant to applications in which high frequency selectivity is more important than wide data bandwidth. Examples include low-rate telemetry, narrowband sensing, low-power wireless links, instrumentation, frequency-selective monitoring, and narrowband communication systems, including telemetry and tele-command channels described in narrowband communication standards [31, 32]. In these systems, reducing the occupied bandwidth can improve spectral concentration and may help reject adjacent-channel interference, provided that the corresponding insertion-loss and dynamic-range requirements can be satisfied [33–39].

From a filter-design perspective, the proposed method provides a useful way to estimate the number of cascades needed to approach a target bandwidth. For example, the two-term power-law model developed in Section 7 can be used as a preliminary design equation:

$$\mathrm{BW}_{3\mathrm{dB}}(K) = 8.809K^{-0.5349} - 0.4827, \tag{56}$$

where the bandwidth is expressed in megahertz. The inverse form of this equation provides a direct estimate of the required cascade order for a desired bandwidth. This is useful in early-stage design because it allows the designer to estimate whether a target bandwidth is achievable within an acceptable cascade order and loss budget.

Nevertheless, the high-order narrowband and ultra-narrowband cases should be interpreted with caution. The extremely high side-lobe-rejection values reported for large K arise from repeated multiplication in the ideal linear magnitude domain followed by conversion to decibels. In practical measurements, such large rejection values would be limited by the noise floor, instrumentation dynamic range, electromagnetic feedthrough, substrate loss, electrode reflections, impedance mismatch, and fabrication imperfections. Therefore, the high-order results should be viewed as model-based indicators of the response trend rather than direct predictions of measurable device rejection.

The insertion-loss penalty is the most important practical constraint for narrowband and ultra-narrowband operation. As the cascade order increases, the passband becomes narrower and the side lobes are suppressed more strongly, but the peak response level decreases substantially. In a real system, this would reduce the available output signal and could degrade the signal-to-noise ratio unless additional gain, low-noise amplification, impedance matching, or compensation techniques are introduced. Therefore, the usable cascade order would be determined not only by the target bandwidth but also by the allowable insertion loss and the minimum detectable signal level.

Second-order acoustic and electromagnetic effects are also expected to become more important at high cascade orders. The present work uses the delta-function model and includes only a simplified treatment of triple-transit interference. A fabricated SAW filter would also be influenced by electromagnetic feedthrough, electrode reflections, diffraction, bulk-wave excitation, propagation loss, and loading effects [6–8, 13]. These effects may introduce passband ripple, spurious responses, additional attenuation, and deviations from the ideal model-predicted bandwidth. Therefore, future work should incorporate more complete physical models before the high-order predictions are translated into device-level design rules.

The results also suggest that the proposed method may be useful as a design-screening tool for narrowband SAW-filter synthesis. Rather than fabricating or fully simulating many possible physical layouts, a designer can first use the cascaded-response model to estimate the theoretical relationship between bandwidth, side-lobe rejection, and loss. Once a suitable range of cascade orders is identified, more detailed modeling methods, such as coupling-of-modes analysis, P-matrix modeling, or finite-element simulation, can be used to evaluate the most promising designs more accurately [6, 8].

For ultra-narrowband applications, the model-predicted bandwidths in the hertz range should be interpreted as theoretical response-shaping limits under ideal assumptions, with potential relevance to ultra-narrowband IoT and low-probability-of-intercept communication concepts [40–43]. Achieving such bandwidths in practice would require very high frequency stability, extremely low phase noise, accurate fabrication control, and careful thermal compensation. In addition, the very large attenuation associated with high cascade orders would likely require active compensation or a different physical implementation strategy. Thus, the ultra-narrowband results are best understood as evidence of the mathematical trend of the proposed method, not as immediate practical performance claims.

In summary, the cascaded frequency-response method provides a clear and analytically tractable framework for studying narrowband and ultra-narrowband SAW-filter behavior. The method shows that repeated response multiplication can strongly suppress side lobes and reduce 3-dB bandwidth, while the regression models provide compact equations for estimating the required cascade order. However, practical realization requires balancing the desired bandwidth and rejection against insertion loss, noise floor, fabrication tolerance, and second-order acoustic effects. This balance defines the main engineering challenge for applying the proposed method to real narrowband and ultra-narrowband SAW-filter systems.

Therefore, the narrowband behavior predicted by the proposed cascaded-response method may be relevant to portable biosensing, NB-IoT, and IoMT communication scenarios, where selective signal conditioning, reliable transmission, reduced interference, and low-power connectivity are important design considerations [44–47]. The relevance of compact and selective RF components is further supported by recent studies on 5G/B5G antennas and 5G smart-application requirements, where bandwidth, data rate, latency, and communication reliability are key design concerns [48, 49].

10 Limitations and Future Work

Although the proposed cascaded frequency-response method provides clear insight into the relationship between cascade order, side-lobe rejection, 3-dB bandwidth, and insertion loss, several limitations must be acknowledged. The present study is based on the delta-function model, which is a useful first-order analytical tool for estimating the frequency response of IDT-based SAW filters. However, this model does not fully represent all physical mechanisms that affect fabricated SAW devices. In particular, electromagnetic feedthrough, electrode reflections, diffraction, bulk-wave excitation, acoustic propagation loss, impedance loading, and substrate-related parasitic effects are not explicitly included in the present formulation [6–8, 13].

The second limitation concerns the treatment of loss. In this work, the cascaded response is generated through repeated multiplication of the output-IDT frequency response. This approach is suitable for studying the theoretical selectivity trend, but it leads to a rapid reduction in peak response level as the cascade order increases. Therefore, the very high side-lobe-rejection values predicted at large cascade orders should be interpreted as ideal model-based results rather than directly measurable device performance. In a practical measurement environment, the achievable rejection would be limited by the noise floor, instrumentation dynamic range, electromagnetic coupling, fabrication tolerance, and parasitic acoustic responses.

A third limitation is that the current study focuses only on uniformly apodized rectangular-window IDTs. This choice is useful because it provides a simple baseline structure and makes the effect of frequency-response cascading easy to observe. However, rectangular weighting is known to produce relatively high side-lobe levels compared with tapered window functions [9]. Future work should therefore extend the proposed cascaded-response methodology to other IDT apodization profiles, including Hamming, Hanning, Kaiser, Blackman, Dolph–Chebyshev, and other optimized weighting functions. Such apodization schemes may reduce the required cascade order for a given side-lobe-rejection target and may help mitigate the insertion-loss penalty.

The fourth limitation is that the regression models developed in this work are empirical fits to the simulated data. The linear side-lobe-rejection model and the nonlinear bandwidth models are accurate within the fitted range of cascade orders, but they should not be interpreted as universal physical laws. Extrapolation to very high cascade orders can indicate the expected trend, but it must be treated cautiously because additional loss mechanisms and second-order effects become increasingly important. Therefore, future work should validate the regression equations using more complete modeling techniques, such as coupling-of-modes analysis, P-matrix modeling, equivalent-circuit modeling, or finite-element simulation [6, 8].

Future research should also investigate the physical implementation of the proposed concept. The present work treats cascading as a frequency-domain synthesis operation rather than as a fabricated multi-stage SAW structure. A practical implementation would require careful consideration of acoustic and electrical loading between stages, impedance matching, packaging effects, gain compensation, and thermal stability. In addition, if amplification is introduced to compensate for the loss penalty, the effects of amplifier noise, linearity, phase response, and stability must be included in the system-level design.

Experimental validation is another important direction. Fabricating a representative SAW filter and comparing measured responses with the predicted cascaded responses would allow the model accuracy to be assessed under real fabrication and measurement conditions. Such validation would also help determine the practical cascade-order range over which the proposed method remains useful. Measured data could then be used to refine the regression models and to include correction factors for propagation loss, electrode reflections, impedance mismatch, and process variation.

In summary, the present work establishes the theoretical and simulation-based foundation of cascaded frequency-response synthesis for SAW-filter selectivity enhancement. Future work should focus on incorporating more complete physical effects, extending the method to alternative apodization functions, validating the method experimentally, and developing practical implementation strategies that balance side-lobe rejection, bandwidth sharpening, insertion loss, and system-level noise performance.

11 Conclusion

This paper presented a cascaded frequency-response method for improving the selectivity of uniformly apodized SAW filters. A rectangular-window SAW filter composed of a 7-electrode input IDT and a 40-electrode output IDT was modeled using the delta-function approximation. The baseline response was obtained from the product of the input- and output-IDT responses, and higher-order cascaded responses were then generated by repeatedly multiplying the composite response by the output-IDT response.

The simulated results showed that increasing the cascade order significantly improves side-lobe rejection and reduces the 3-dB bandwidth. These improvements are relative to the ideal simulated magnitude response and should be interpreted together with the corresponding peak-response degradation. For cascade orders from $K = 1$ to $K = 50$, the center frequency remained approximately constant near 162 MHz after the first cascade. Over the same range, the side-lobe rejection increased from 8.24 dB to 575.80 dB, while the 3-dB bandwidth decreased from 8.70 MHz to 0.549 MHz. These results confirm that repeated response multiplication can strongly suppress side-lobe regions and sharpen the main passband in the ideal simulation model.

The results also revealed a clear selectivity–loss trade-off. Although side-lobe rejection and bandwidth selectivity improve with increasing cascade order, the peak response level decreases substantially. The peak response level changed from approximately -11.31 dB for the baseline response to approximately -305.50 dB after 50 cascades. This indicates that insertion loss is the main practical constraint of the proposed approach, especially when high cascade orders are used.

Regression models were developed to describe the simulated trends and to provide compact performance-prediction tools. The side-lobe rejection was accurately described by a linear model, indicating that each additional cascade contributes an approximately constant improvement in rejection within the simulated range. In contrast, the 3-dB bandwidth followed a nonlinear decreasing trend and was modeled using Gaussian, polynomial, and power-law regression functions. The eight-term Gaussian model provided the highest fitting accuracy, while the two-term power-law model offered the simplest form for early-stage design estimation.

High-order simulations further demonstrated the theoretical ability of the cascaded-response method to produce narrowband and ultra-narrowband responses. However, these results should be interpreted as ideal model-based predictions rather than direct practical device performance. At very high cascade orders, the predicted response would be strongly affected by insertion loss, numerical dynamic range, noise-floor limitations, fabrication tolerance, impedance mismatch, and second-order SAW effects that are not fully included in the delta-function model.

Overall, the proposed cascaded frequency-response method provides a simple and analytically tractable approach for studying SAW-filter selectivity enhancement. The method is useful for early-stage design because it quantifies the relationship between cascade order, side-lobe rejection, 3-dB bandwidth, and insertion loss. The results show that substantial selectivity improvement can be achieved in simulation, but practical implementation requires careful optimization of the loss budget, physical device structure, impedance matching, and second-order acoustic effects. Future extensions using dynamic-range-limited modeling, coupling-of-modes or P-matrix validation, alternative apodization functions, and experimental measurements will be necessary to translate the predicted response-synthesis trends into practical SAW-filter designs.

Acknowledgment

The author would like to acknowledge the support of the Department of Electrical Engineering, College of Engineering, Zarqa University.

References

[1] R. N. Thurston, *Surface Acoustic Wave Devices and Their Applications*. Wiley-IEEE Press, 1993, chapter 4.
[2] C. C. W. Ruppel, "Acoustic wave filter technology—a review," *IEEE Transactions on Ultrasonics, Ferroelectrics, and Frequency Control*, vol. 64, no. 9, pp. 1390–1400, 2017.
[3] T. Bauer, C. Eggs, K. Wagner, and P. Hagn, "A bright outlook for acoustic filtering: A new generation of very low-profile SAW, TC SAW, and BAW devices for module integration," *IEEE Microwave Magazine*, vol. 16, no. 7, pp. 73–81, 2015.
[4] P. Chen, G. Li, and Z. Zhu, "Development and application of SAW filter," *Micromachines*, vol. 13, no. 5, p. 656, 2022.
[5] R. M. White and F. W. Voltmer, "Direct piezoelectric coupling to surface elastic waves," *Applied Physics Letters*, vol. 7, no. 12, pp. 314–316, 1965.
[6] D. P. Morgan, *Surface Acoustic Wave Filters: With Applications to Electronic Communications and Signal Processing*, 2nd ed. Academic Press, 2007, chapter 5, pp. 121–134.
[7] C. K. Campbell, *Surface Acoustic Wave Devices for Mobile and Wireless Communications*. Academic Press, 1998, chapter 3, Section 3.4.
[8] K.-y. Hashimoto, *Surface Acoustic Wave Devices in Telecommunications: Modelling and Simulation*. Berlin, Heidelberg: Springer, 2000, chapter 3: Interdigital Transducers.
[9] F. J. Harris, "On the use of windows for harmonic analysis with the discrete fourier transform," *Proceedings of the IEEE*, vol. 66, no. 1, pp. 51–83, 1978.
[10] Lee, H. Kim, and J. Park, "Apodization and window-function techniques for SAW filters," *IEEE Transactions on Microwave Theory and Techniques*, vol. 58, no. 9, pp. 2525–2534, Sep. 2010.
[11] J. G. Gwilliam, "Multistage SAW filter design for ultra-narrow bandwidth," in *IEEE MTT-S International Microwave Symposium Digest*, 1999, pp. 357–360.
[12] G. Liu, Y. Zhang, and M. Zhang, "Iterative design of narrow-band SAW filters using cascaded IDTs," *Sensors and Actuators A: Physical*, vol. 186, pp. 56–63, 2012.
[13] S. Datta, *Surface Acoustic Wave Devices*. Englewood Cliffs, NJ, USA: Prentice-Hall, 1986.
[14] P. J. Kelley, *Fundamentals of SAW Devices*, 2nd ed. Wiley-IEEE Press, 2014, chapter 7.
[15] A. M. Ghosh, "Finite-element modelling of uniformly apodised SAW filters," in *Proceedings of the IEEE International Conference on RF and Microwave*, 2015, pp. 1–5.
[16] J. D. Simons and H. J. Cheng, "Analysis of SAW filters using the delta-function method," *IEEE Transactions on Ultrasonics, Ferroelectrics, and Frequency Control*, vol. 44, no. 2, pp. 352–361, Mar. 1997.

[17] C. Herring, *Acoustic Wave Devices: Modeling and Design*. Artech House, 1995, section 2.4: IDT Edge Charge Model.
[18] C. K. Campbell, *Surface Acoustic Wave Devices and Their Signal Processing Applications*. San Diego, CA, USA: Academic Press, 1989.
[19] J. D. Simons and H. J. Cheng, "Triple transit interference in surface acoustic wave filters," *IEEE Transactions on Ultrasonics, Ferroelectrics, and Frequency Control*, vol. 44, no. 2, pp. 352–361, Mar. 1997.
[20] The MathWorks, Inc., *MATLAB Documentation*, The MathWorks, Inc., Natick, MA, USA, 2024, available online: https://www.mathworks.com/help/matlab/.
[21] N. R. Draper and H. Smith, *Applied Regression Analysis*, 3rd ed. New York, NY, USA: Wiley, 1998.
[22] D. C. Montgomery, E. A. Peck, and G. G. Vining, *Introduction to Linear Regression Analysis*, 5th ed. Hoboken, NJ, USA: Wiley, 2012.
[23] J. W. Hartley, "Statistical regression analysis for RF device characterisation," *IEEE Transactions on Microwave Theory and Techniques*, vol. 55, no. 5, pp. 1220–1229, May 2007.
[24] The MathWorks, Inc., *Curve Fitting Toolbox User's Guide*, The MathWorks, Inc., Natick, MA, USA, 2024.
[25] D. C. Henderson, *Applied Statistics for Engineers and Scientists*, 3rd ed. Wiley, 2019, chapter 7, p. 215.
[26] G. F. Quintana and J. M. Garcia, "Multivariate gaussian modelling of frequency-response data," *IEEE Access*, vol. 9, pp. 112 345–112 357, 2021.
[27] J. A. Hernandez and L. M. Lopez, "High-order polynomial regression for RF filter parameter extraction," *Microwave and Optical Technology Letters*, vol. 62, no. 4, pp. 392–399, 2020.
[28] The MathWorks, Inc., *MATLAB R2024b Fit Type power2 Documentation*, The MathWorks, Inc., Natick, MA, USA, 2024.
[29] National Instruments, *LabVIEW User Manual*, National Instruments, Austin, TX, USA, 2024.
[30] ——, *LabVIEW 2024 Development Guide: Building Graphical User Interfaces for RF Modelling*, National Instruments, Austin, TX, USA, 2024.
[31] ITU-R, "Recommendation M.1457: Characteristics of narrow-band and broadband transmission systems," International Telecommunication Union, Tech. Rep., 2020.
[32] ETSI, "EN 300 220-2: Narrow-band communication for telemetry and tele-command," European Telecommunications Standards Institute, Tech. Rep., 2015.
[33] B. Sklar, *Digital Communications: Fundamentals and Applications*, 2nd ed. Upper Saddle River, NJ, USA: Prentice Hall PTR, 2001.
[34] T. S. Rappaport, *Wireless Communications: Principles and Practice*, 2nd ed. Upper Saddle River, NJ, USA: Prentice Hall PTR, 2002, section 5.4.
[35] A. Goldsmith, *Wireless Communications*. Cambridge, UK: Cambridge University Press, 2005.
[36] H. L. Van Trees, *Detection, Estimation, and Modulation Theory, Part I*. Wiley-Interscience, 2001, energy concentration in narrow bands.
[37] M. K. Simon, *Digital Communication Techniques: From Theory to Practice*. Cambridge University Press, 2005, chapter 6: Fading and bandwidth.
[38] ARRL, *The ARRL Handbook for Radio Communications*. ARRL, 2022, section 9.2: Narrow-band FM.
[39] M. M. Mishra, *Principles of Data Communications and Networking*, 2nd ed. Wiley, 2002, dial-up bandwidth.
[40] P. M. K. K. G. Bansal, "Ultra-narrow-band communication for IoT," *IEEE Internet of Things Journal*, vol. 7, no. 5, pp. 4201–4210, May 2020.
[41] J. R. Khaligh, *IoT in the Ultra-Narrow-Band Regime*. Springer, 2021, chapter 3.
[42] Sigfox, "UNB for massive IoT: 100 hz channel design and performance," Sigfox, White Paper, 2022.
[43] A. R. Said, "Low-probability-of-intercept ultra-narrow-band waveforms for defense applications," *IEEE Transactions on Aerospace and Electronic Systems*, vol. 58, no. 3, pp. 1918–1927, Mar. 2022.
[44] A. A. Shati, F. Al-Dolaimy, M. Y. Alfaifi, R. Z. Sayyed, S. Mansouri, Z. Aminov, R. Alubady, K. Gandla, A. H. R. Alawady, and A. H. Alsaalamy, "Recent advances in using nanomaterials for portable biosensing platforms towards marine toxins application: Up-to-date technology and future prospects," *Microchemical Journal*, vol. 195, p. 109500, 2023.
[45] S. F. Jabbar, N. S. Mohsin, J. F. Tawfeq, P. S. Joseph Ng, and A. L. Khalaf, "A novel data offloading scheme for QoS optimization in 5G-based internet of medical things," *Bulletin of Electrical Engineering and Informatics*, vol. 12, no. 5, pp. 3124–3133, 2023.
[46] ITU-R, "Recommendation M.2083: IoT technologies: Deployment and performance," International Telecommunication Union, Tech. Rep., 2019, UHF/VHF LPWAN allocations.
[47] 3GPP, "TS 36.331: Narrowband IoT (NB-IoT) radio access network architecture," 3rd Generation Partnership Project, Tech. Rep., 2021.
[48] H. Attar, R. S. Agieb, A. Amer, A. Solyman, and M. S. Aziz, "Microstrip patch antenna design and implementation for 5G/B5G applications," in *2022 International Engineering Conference on Electrical, Energy, and Artificial Intelligence (EICEEAI)*. IEEE, 2023, pp. 1–6.
[49] H. Attar, H. Issa, J. Ababneh, M. Abbasi, A. A. A. Solyman, M. R. Khosravi, and R. S. Agieb, "5G system overview for ongoing smart applications: Structure, requirements, and specifications," *Computational Intelligence and Neuroscience*, vol. 2022, p. 2476841, 2022.

Haitham Issa received his Ph.D. in Communications and Information systems from Zhejiang University, Hangzhou, China, in 2002. He is currently teaching in the Department of Electrical Engineering in Zarqa University, Zarqa, Jordan. His current research interests include image processing, signal Processing, pattern recognition, machine learning, communication, and renewable energy.

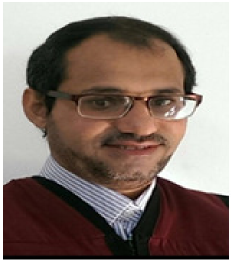

Hani Attar received his Ph.D. from the Department of Electrical and Electronic Engineering, University of Strathclyde, United Kingdom in 2011. Since 2011, he has been working as a researcher of electrical engineering and energy systems. Dr. Attar is now a university lecturer at Zarqa University, Jordan. His research interests include renewable energy systems, efficient designs, and Wireless Communications.

Jafar Ababneh received the B.Sc. degree in telecommunication engineering, in 1991, the M.Sc. degree in 2005, and the Ph.D. degree, in 2009. He is an Associate Professor. In 2009, he joined WISE University as the head of computer information and network systems in information technology (IT) till 2/2022. He was the dean of the IT faculty, WISE University, from August 2015 to November 2020, In 2022, he joined Abdul Aziz Al Ghurair School of Advanced Computing (ASAC), LUMINUS Technical University College (LTUC). He has published many research papers, book chapters, and books in international refereed journals and conferences. His research interests include congestion and network performance, wireless and mobile network, encryption and Information Security, Wireless Sensor Networks (WSNs), Artificial Intelligence, data mining and retrieving information, cloud computing and E-learning.

Zakaria Che Muda is a Professor in Civil Engineering at INTI International University, Malaysia. He received his PhD in Built Environment from the University of Malaya and his MSc in Structural Engineering from the University of Manchester. His research focuses on structural engineering, numerical and reliability-based analysis, fibre-reinforced concrete, sustainable lightweight concrete, energy-efficient buildings, and advanced AI applications in engineering. He has published more than 100 papers in international journals.

Ismail A. M. Elhaty is an Assistant Professor in the Department of Nutrition and Dietetics, Faculty of Health Sciences, at Istanbul Gelisim University, Istanbul, Turkey. He earned his bachelor's, master's, and doctoral degrees from United Arab Emirates University. His research interests include plant biochemistry, analytical chemistry, organic chemistry, and environmental pollution.

Eman Salah Abass Gad Assistant Professor at AlRyada University, specializes in cybersecurity, AI, and wireless communications. She holds a Ph.D. in Electronics and Communication Engineering from Ain Shams University (MIMO systems for next-gen wireless). Her awards include innovations in smart agriculture and sustainable engineering.

Ramy M. Bahy received the Ph.D. degree in Electrical Engineering from the Military Technical College, Cairo, Egypt, in 2012. His research interests include image and video processing, particularly compression, registration, fusion, and enhancement, with special emphasis on super-resolution techniques. He is also interested in hardware-software interfacing for navigation systems aided by image and video processing, as well as the application of image and video processing in simulators.